

# Internal motions in OB-associations with *Gaia* DR2

A.M.Melnik\* and A.K. Dambis

*Sternberg Astronomical Institute, Lomonosov Moscow State University, Universitetskii pr. 13, Moscow, 119991 Russia*

Accepted 2020 February 11. Received 2020 January 17; in original form 2019 June 6

## ABSTRACT

We study the motions inside 28 OB-associations with the use of *Gaia* DR2 proper motions. The average velocity dispersion calculated for 28 OB-associations including more than 20 stars with *Gaia* DR2 proper motion is  $\sigma_v = 4.5 \text{ km s}^{-1}$ . The median virial and stellar masses of OB-associations are  $M_{vir} = 8.9 \times 10^5$  and  $M_{st} = 8.1 \times 10^3 M_{\odot}$ , respectively. The median star-formation efficiency in parent giant molecular clouds appears to be  $\epsilon = 1.2$  per cent. *Gaia* DR2 proper motions confirm the expansion in the Per OB1, Car OB1 and Sgr OB1 associations found earlier with *Gaia* DR1 data. We also detect the expansion in Gem OB1, Ori OB1 and Sco OB1 associations which became possible for the first time now when analyzed with *Gaia* DR2 proper motions. The analysis of the distribution of OB-stars in the Per OB1 association shows the presence of a shell-like structure with the radius of 40 pc. Probably, the expansion of the Per OB1 association started with the velocity greater than the present-day expansion velocity equal to  $5.0 \pm 1.7 \text{ km s}^{-1}$ .

**Key words:** Galaxy: kinematics and dynamics – open clusters and associations

## 1 INTRODUCTION

The second intermediate *Gaia* data release (*Gaia* DR2), which is based on the data collected during the first 1.8 yr of *Gaia* mission, provides proper motions for more than 1.3 billion stars with a characteristic accuracy of  $\sim 0.1 \text{ mas yr}^{-1}$  (Brown et al. 2018; Lindegren et al. 2018; Katz et al. 2018). The main achievement of *Gaia* DR2 is the large number of stars with high-precision astrometric data.

The first *Gaia* data release (*Gaia* DR1) contains *Tycho-Gaia* Astrometric Solution (TGAS, Michalik, Lindegren & Hobbs 2015; Lindegren et al. 2016) for  $\sim 2$  million stars based on positions spanning a 24 yr time interval between Hipparcos (ESA 1997) and *Gaia* (Gaia Collaboration et al. 2016a) measurements.

Melnik & Dambis (2017) used *Gaia* DR1 (TGAS) data to identify 500 stars in OB-associations. These stars have their first-epoch positions determined by the Hipparcos catalog (ESA 1997), which provides the accuracy of TGAS proper motions of  $\sim 0.06 \text{ mas yr}^{-1}$ . The average one-dimensional velocity dispersion inside 18 OB-associations with more than 10 TGAS stars appeared to be  $\sigma_v = 3.9 \text{ km s}^{-1}$ . Precise *Gaia* DR1 (TGAS) proper motions allowed us to find the expansion in the Per OB1, Car OB1 and Sgr OB1 associations determined at significance level  $P > 2.5\sigma$  (Melnik & Dambis 2017).

As for the motion of OB-associations as whole entities, the results obtained with *Gaia* DR1 and *Gaia* DR2 data are in good agreement. The median velocities of OB-associations derived from *Gaia* DR1 and *Gaia* DR2 proper motions differ on average by  $2 \text{ km s}^{-1}$ . The parameters of the rotation curve calculated with proper motions from *Gaia* DR1 and *Gaia* DR2 are consistent within the errors (Melnik & Dambis 2017; Melnik 2019).

OB-associations are sparse groups of O and B stars (Ambartsumian 1949). They are supposed to be born in giant molecular clouds (Elmegreen 1983; Zinnecker & Yorke 2007). There is extensive evidence that giant molecular clouds are in a state close to virial equilibrium (Larson 1981; Krumholz, Matzner & McKee 2006; Kauffmann, Pillai & Goldsmith 2013; Chen et al. 2019). The expected sizes and masses of giant molecular clouds are 10–80 pc and  $10^5 - 2 \cdot 10^6 M_{\odot}$ , respectively (Sanders, Scoville & Solomon 1985). The estimates of the average efficiency of star formation,  $\epsilon$ , in giant molecular clouds defined as the ratio of the total mass of stars born inside a cloud to the initial gas mass lies in the range of 0.1–10 percent (Myers et al. 1986; Evans et al. 2009; Garcia et al. 2014). The median star-formation efficiency determined for 18 OB-associations with more than 10 TGAS stars appears to be 2.1 per cent (Melnik & Dambis 2017).

The radiation of massive stars creates HII regions, which can destroy molecular clouds (McKee 1989; Franco, Shore & Tenorio-Tagle 1994; Colin, Vazquez-Semadeni & Gomez 2013;

\* E-mail: anna@sai.msu.ru

Kim, Kim & Ostriker 2016). If a gas cloud loses more than 50 per cent of its mass in a time less than one crossing time, then the system becomes unbound (Hills 1980). But if the mass is ejected slowly then the system can form an expanding OB-association with a bound cluster in its centre (Kroupa, Aarseth & Hurley 2001; Boily & Kroupa 2003a,b; Baumgardt & Kroupa 2007).

The catalog by Blaha & Humphreys (1989) comprises 91 OB-association located within  $\sim 3$  kpc of the Sun. Melnik & Efremov (1995) found that many of OB-associations identified by Blaha & Humphreys (1989) include several centres of concentration.

The study by Blaauw (1964) stimulated the interest in the search of expanding OB-associations. Several methods have been proposed for determining the parameters of expansion in stellar groups (Brown, Dekker & de Zeeuw 1997; Madsen, Dravins & Lindegren 2002). Many studies of expansion of OB-associations based on *Gaia* data have been undertaken in the last few years. Kounkel et al. (2018) studied the kinematics of the Ori OB1 association and found significant expansion in only one subgroup inside it. Cantat-Gaudin et al. (2019) studied the Vela OB2 association and detected expansion in all seven detected subgroups. Wright & Mamajek (2018) investigated the Sco OB2 association and found no evidence of expansion inside three selected subgroups. Ward & Kruijssen (2018) identified 18 associations on the basis of their original method and reported that none of them shows evidence of expansion.

Here we do not use *Gaia* DR2 parallaxes for stars of OB-associations because they seem to need some correction of their zero point, moreover, different studies give different values for this correction (Lindegren et al. 2018; Arenou et al. 2018; Stassun & Torres 2018; Riess et al. 2018; Yalyalieva et al. 2018, and other papers). Exception is the Ori OB1 association for which trigonometric and photometric methods give the same distance of 0.4 kpc. Note that associations located at the distances of  $\sim 2$  kpc do not show such an agreement. We also do not consider *Gaia* DR2 line-of-sight velocities because they are measured for only 7 per cent of stars of OB-associations.

In this paper we study the internal motions of young stars inside OB-associations as derived from *Gaia* DR2 proper motions. Section 2 describes the catalog of stars in OB-associations with *Gaia* DR2 astrometric and photometric data. Section 3 analyzes velocity dispersion inside OB-associations, determines the virial and stellar masses of OB-associations, estimates the star-formation efficiency in giant molecular clouds, studies the expansion of OB-associations and the role of shell-like structures. Section 4 discusses the results and formulates the main conclusions.

## 2 DATA

The catalog by Blaha & Humphreys (1989) includes 2209 high-luminosity stars of OB-associations, 2007 of them have been identified with *Gaia* DR2 catalog and 1990 (90 per cent) have *Gaia* DR2 proper motions.

We identified members of OB-associations from the catalog by Blaha & Humphreys (1989) with *Gaia* DR2 stars based on the proximity of stellar coordinates and visual magnitudes. The coordinates in the catalog by

Blaha & Humphreys (1989) are given with small accuracy and therefore we also invoke data from Strasbourg astronomical Data Center.

We cross-matched the list of Blaha & Humphreys (1989) with *Gaia* DR2 catalog using a matching radius of 3 arcsec and the magnitude tolerance of  $|G_{BH} - G| < 3^m$  which gave us matches for a total of 2007 stars. Out of them the 3-arcsec matches were unique for 1873 stars, 131 stars had two matches, and 3 stars had three matches. For stars with unique matches the matching distance did not exceed 0.5 arcsec (the median value is 0.051 arcsec), for stars with 2 or 3 matches the distance for the closest match did not exceed 0.19 arcsec (the median value is 0.048 arcsec), the median distances to the second- and third matches is 2.01 arcsec, respectively. We therefore adopted all matches where they were unique and adopted the closest match in the remaining cases.

We also compare *Gaia* *G*-band magnitudes with the *G*-band magnitudes ( $G_{BH}$ ) predicted for stars from Blaha & Humphreys (1989) list based on the *B*- and *V*-band data provided in it. The predicted *G*-band values were derived on the basis of an empirical relation involving  $(B - V)$  color indices and *V*-band magnitudes (Jordi et al. 2010):

$$G_{BH} = V - 0.0424 - 0.0851(B - V) - 0.3348(B - V)^2 + 0.0205(B - V)^3. \quad (1)$$

Table 1 (available in the online version of the paper) lists the kinematic and photometric data for stars in OB-associations obtained with *Gaia* DR2. It presents the name of a star, the name of the OB-association to which it is assigned, spectral type of the star, its luminosity class and visual magnitude,  $m_v$ , which all are taken from the catalog by Blaha & Humphreys (1989). We also show the heliocentric distance to the OB-association by Blaha & Humphreys (1989),  $r_{BH}$ , reduced to the short distance scale,  $r = 0.8 r_{BH}$  (Sitnik & Melnik 1996; Dambis, Melnik & Rastorguev 2001; Melnik & Dambis 2009). Table 1 also represents *Gaia* DR2 data: equatorial coordinates,  $\alpha$  and  $\delta$ , of the star, its Galactic coordinates,  $l$  and  $b$ , the magnitude in the *G*-band, the parallax,  $\pi$ , proper motions along *l*- and *b*-directions,  $\mu_l$  and  $\mu_b$ , and their errors,  $\varepsilon_\pi$ ,  $\varepsilon_{\mu_l}$  and  $\varepsilon_{\mu_b}$ . It also lists the number of visibility periods,  $n_{vis}$ , of the star, i. e. the number of groups of observations separated from each other by at least 4 days (Arenou et al. 2018), and the re-normalised unit weight errors (RUWE), which measure how well the *Gaia* observations agree with the five-parameter single-star model and whose large value (RUWE > 1.4) could indicate an astrometric binary (Lindegren 2018, 2019). For completeness we also added to Table 1 the stellar line-of-sight velocities,  $V_r$ , and their errors,  $\varepsilon_{V_r}$ , taken from the catalog by Barbier-Brossat & Figon (2000), which are available for 52 per cent of stars of OB-associations. Here we will consider the refined sample of stars in OB-associations including 1771 stars with  $n_{vis} > 8$  and RUWE < 1.4. Of 219 excluded stars, 174 stars have RUWE  $\geq 1.4$  and 45 objects have  $n_{vis} \leq 8$ .

### 3 RESULTS

#### 3.1 Velocity dispersion inside OB-associations

Let us consider the motions of stars in OB-associations in the sky plane. The velocity components of a star along  $l$ - and  $b$ -directions,  $v_l$  and  $v_b$ , are calculated as follows:

$$v_l = 4.74 \mu_l r, \quad (2)$$

$$v_b = 4.74 \mu_b r, \quad (3)$$

where  $r$  is the heliocentric distance of the association but  $\mu_l$  and  $\mu_b$  are proper motions in  $\text{mas yr}^{-1}$ . The factor  $4.74 \times r$  (kpc) transformers units of  $\text{mas yr}^{-1}$  into  $\text{km s}^{-1}$ .

We determine the standard deviations,  $\sigma_{vl}$  and  $\sigma_{vb}$ , of velocity components,  $v_l$  and  $v_b$ , in an association as half of the velocity interval,  $\Delta v_l$  and  $\Delta v_b$ , including central 68 per cent of member stars with known *Gaia* DR2 proper motions. These robust estimates of the velocity dispersion allow us to minimize the contribution of outliers.

The average uncertainty in determination of proper motions of stars of OB-associations in *Gaia* DR2 is  $0.086 \text{ mas yr}^{-1}$ , which corresponds to the uncertainty in the sky-plane velocity of stars at the distance of  $r = 1 \text{ kpc}$  equal to  $0.4 \text{ km s}^{-1}$ .

Figure 1 compares the dispersions of stellar proper motions inside OB-associations derived with *Gaia* DR1 (TGAS) and *Gaia* DR2 data,  $\sigma_{\mu 1}$  and  $\sigma_{\mu 2}$ , respectively. We can see that the dispersions obtained with *Gaia* DR2 proper motions are systematically larger than those calculated with *Gaia* DR1 data. The linear relation between them is  $\sigma_{\mu 2} = 1.09 \pm 0.08 \sigma_{\mu 1}$ . Here we consider 13 OB-associations with  $\sigma_{\mu 2} < 2.5 \text{ mas yr}^{-1}$  and including more than 10 stars common for the Hipparcos, *Gaia* DR1 and *Gaia* DR2 catalogs.

Table 2 lists the average standard deviations,  $\overline{\sigma_{vl}}$  and  $\overline{\sigma_{vb}}$ , of velocities,  $v_l$  and  $v_b$ , inside OB-associations, calculated for different samples of member stars with *Gaia* proper motions.

We corrected the velocity dispersions inside OB-associations for the inflationary-effect of measurement errors by the following way:

$$\sigma_{vl}^2 = \sigma_{l, obs}^2 - (4.74 r \varepsilon_{\mu l})^2, \quad (4)$$

$$\sigma_{vb}^2 = \sigma_{b, obs}^2 - (4.74 r \varepsilon_{\mu b})^2, \quad (5)$$

where  $\varepsilon_{\mu l}$  and  $\varepsilon_{\mu b}$  are the average errors in determination of proper motions inside an association in the  $l$ - and  $b$ -directions, respectively. Table 2 also presents the average velocity dispersions derived for both  $l$ - and  $b$ -directions:

$$\overline{\sigma_v} = (\overline{\sigma_{vl}} + \overline{\sigma_{vb}})/2; \quad (6)$$

and the root-mean-square errors in determination of the average velocity dispersions. Table 2 also lists the minimal number of stars,  $n_{\mu}$ , with known *Gaia* proper motions, which an association must include for it to be considered in our study, and the number of associations in the sample,  $n$ . The comments indicate the criteria for selection of stars in associations. The first four rows are related to *Gaia* DR2 proper motions while the fifth row presents quantities derived from *Gaia* DR1 data. The first and second rows represent samples including associations with more than  $n_{\mu} > 20$  and  $n_{\mu} > 10$  *Gaia* DR2 stars, respectively. The third, fourth and fifth

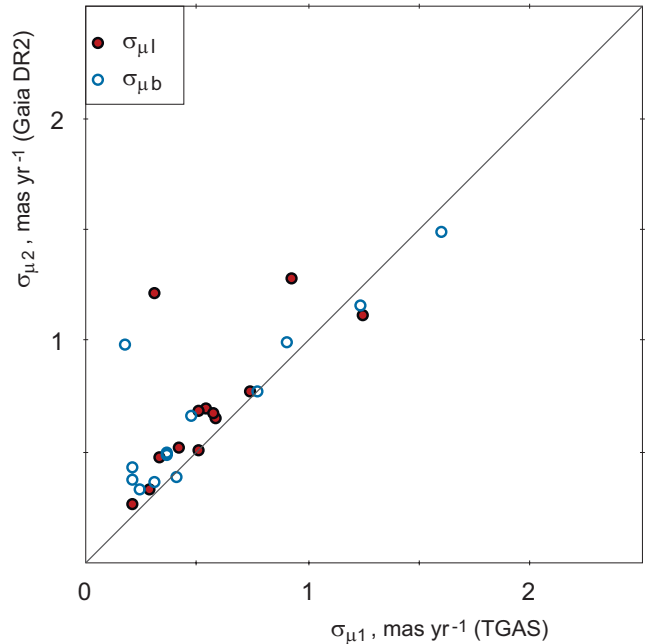


**Figure 1.** Comparison of the dispersions of the proper motions of stars inside OB-associations derived with *Gaia* DR2 and with *Gaia* DR1 (TGAS) data. The solid line shows the bisectrix. We can see that the dispersions obtained with *Gaia* DR2 proper motions are systematically larger than those calculated with *Gaia* DR1. The Cyg OB7 association with the dispersions  $\sigma_{\mu 1} = 3.76$  and  $\sigma_{\mu 2} = 4.51 \text{ mas yr}^{-1}$  is located beyond the limits of the plot.

rows lists quantities derived only for stars common for Hipparcos and *Gaia* catalogs. The selection of Hipparcos stars in *Gaia* DR1 (TGAS) data allows us to use the most precise proper motions (fifth row).

Table 2 suggests that all estimates of the velocity dispersions inside OB-associations derived from *Gaia* DR2 data (the first four rows) are greater than those obtained with *Gaia* DR1 (the bottom row). However, the statistical significance of this predominance is not large (just  $P \sim 1 \sigma$ ). For example, the average velocity dispersion  $\overline{\sigma_v}$  calculated for 28 associations with more than  $n_{\mu} > 20$  *Gaia* DR2 proper motions (first row) amounts to  $4.46 \pm 0.30 \text{ km s}^{-1}$  but  $\overline{\sigma_v}$  computed for *Gaia* DR1 data is only  $3.54 \pm 0.49 \text{ km s}^{-1}$  (fifth row). Note that the velocity dispersions shown in the fourth and fifth rows are derived on the basis of the same sample of stars, and their comparison gives the most convincing argument that the velocity dispersion,  $\overline{\sigma_v}$ , obtained with *Gaia* DR2 data is greater than  $\overline{\sigma_v}$  calculated with *Gaia* DR1 data at a significance level of  $P \sim 1 \sigma$ .

We excluded Cep OB1 ( $r = 2.8 \text{ kpc}$ ), NGC 2439 ( $r = 3.5 \text{ kpc}$ ) and R 103 ( $r = 3.2 \text{ kpc}$ ) associations from consideration because of their distant location from the Sun ( $r > 2.8 \text{ kpc}$ ), which results in increased probability of wrong membership. Moreover, the Cep OB1 and NGC 2439 associations are very elongated in the  $l$ -direction, the ratio of their sizes in the  $l$ - and  $b$ -direction exceeds  $d_l/d_b > 2$  which suggests that they can include a chain of OB-associations. The R 103 association has too large velocity dispersion,  $\sigma_{vl} = 21 \text{ km s}^{-1}$ , and seems to be strongly contaminated by field stars.

Generally, the observed velocity dispersion inside OB-associations has several sources: turbulent motions inside

giant molecular clouds, in which young stars were born; motions inside binary systems; the uncertainty in the determination of proper motions. However, the contribution of the latter source is insignificant.

Here we suppose that the contribution of binary systems into the velocity dispersion inside OB-associations is small, no greater than  $\sigma_{bn} \sim 1 \text{ km s}^{-1}$ . Some estimates of the binary effect inside OB-associations will be presented in separated paper (Melnik & Dambis 2020).

### 3.2 Efficiency of star formation

Giant molecular clouds, from which OB-associations form, seem to be close to their virial equilibrium. The velocity dispersion of turbulent motions,  $\sigma_t$ , inside OB-association and the radius of association,  $a$ , can be used to estimate the virial masses,  $M_{vir}$ , of OB-associations, which are equal to the masses of their parent molecular clouds:

$$M_{vir} = \frac{5a\sigma_t^2}{G}, \quad (7)$$

where  $a$  is the specific radius of an association. Here we assume  $a$  to be the radius containing central 68 per cent of association member stars. The velocity dispersion of turbulent motions,  $\sigma_t$ , is supposed to be close to the observed velocity dispersion corrected for measurement errors,  $\sigma_v$ :

$$\sigma_t \approx \sigma_v. \quad (8)$$

Another remark is connected with the expansion of the Car OB1 and Per OB1 associations, which had a considerably smaller size some time ago – this seems to be their initial size – so their present-day radius  $a$  must be corrected by a factor:

$$a_c = a\xi, \quad (9)$$

where  $\xi$  is the ratio of the minimum to the present-day radius of an association (see section 3.4, Eq. 29).

We can also calculate the stellar masses of OB-associations,  $M_{st}$ , through the number of stars with masses greater than  $20 M_\odot$ ,  $N_{20}$ . Note that Blaha & Humphreys (1989) considered the catalog of stars in OB-associations to be fairly complete for stars brighter than  $M_{bol} < -7.5^m$ , which corresponds to stars with masses greater than  $\sim 20 M_\odot$  (Bressan et al. 2012). The power-law mass function by Kroupa (2002) calibrated via  $N_{20}$  can be used to estimate the full mass of stars in an association (for more details see Melnik & Dambis 2017).

Table 3 lists the virial and stellar masses,  $M_{vir}$  and  $M_{st}$ , of OB-associations containing more than 20 stars with *Gaia* DR2 proper motions,  $n_\mu > 20$ . It also lists the general parameters of an OB-association: the average Galactic longitude and latitude,  $l$  and  $b$ ; the average heliocentric distance,  $r$ ; the median line-of-sight velocity,  $V_r$ , and the number of stars it is derived from given in parentheses; the specific radius of OB-association,  $a$ ; the number of stars with masses  $M > 20 M_\odot$ ,  $N_{20}$ ; the velocity dispersions in  $l$ - and  $b$ -directions,  $\sigma_{vl}$  and  $\sigma_{vb}$ , and the number of stars with known *Gaia* DR2 proper motions,  $n_\mu$ . Also listed in Table 3 is the average efficiency of star formation,  $\epsilon$ , inside the parent giant molecular cloud:

$$\epsilon = M_{st}/M_{vir}. \quad (10)$$

Table 3 indicates that the star-formation efficiency in OB-associations ranges from 0.1 to 15 per cent. Its median value calculated for 28 OB-associations is  $\epsilon = 1.2$  per cent. The median virial and stellar masses appear to be  $8.9 \times 10^5$  and  $8.1 \times 10^3 M_\odot$ , respectively.

### 3.3 Expansion of OB-associations

We determine possible expansion or compression of OB-associations via parameters  $p_l$  and  $p_b$ :

$$v_l = v_{l0} + p_l r \sin(l - l_0), \quad (11)$$

$$v_b = v_{b0} + p_b r \sin(b - b_0), \quad (12)$$

where  $v_{l0}$  and  $v_{b0}$  are the average velocities of the association;  $l_0$  and  $b_0$  are the coordinates of the centre of the group and parameters  $p_l$  and  $p_b$  characterize expansion (positive values) or compression (negative values) along the  $l$ - or  $b$ -direction, respectively. We solve the systems of Eq. 11 and Eq. 12 for all member stars of an association with known *Gaia* DR2 proper motions to determine the values of  $p_l$  and  $p_b$ .

The observed specific velocities of expansion or compression,  $u_l$  and  $u_b$ , are computed as:

$$u_l = p_l a, \quad u_b = p_b a. \quad (13)$$

The motion of an OB-association as a whole with line-of-sight velocity  $V_r$  can also produce the effect of spurious expansion/compression, which creates the expansion/compression with the specific velocity  $e_1$ :

$$e_1 = -V_r \frac{a}{r}, \quad (14)$$

where  $a$  and  $r$  are the specific radius and heliocentric distance of the OB-association, respectively. The motion of a group toward the Sun ( $V_r < 0$ ) produces spurious expansion ( $e_1 > 0$ ) while the motion away from the Sun ( $V_r > 0$ ) creates spurious compression ( $e_1 < 0$ ). Generally, the observed velocities,  $u_l$  and  $u_b$ , must be corrected for this effect:

$$\tilde{u}_l = u_l - e_1, \quad \tilde{u}_b = u_b - e_1. \quad (15)$$

Here we use the median values of line-of-sight velocities of OB-associations,  $V_r$  (Table 3), which are derived from the velocities of individual stars taken from the catalog by Barbier-Brossat & Figon (2000).

Table 4 lists the parameters of expansion/compression,  $p_l$  and  $p_b$ , the velocities  $u_l$ ,  $u_b$ ,  $e_1$ ,  $\tilde{u}_l$ ,  $\tilde{u}_b$  and their uncertainties for 28 OB-associations containing more than 20 stars with *Gaia* DR2 proper motions. We will discuss only velocities  $\tilde{u}_l$  or  $\tilde{u}_b$  determined at a significance level greater than  $P > 3\sigma$ , which are underlined in Table 4.

Figure 2 shows distribution of observed relative velocities,  $V'_l$  and  $V'_b$ , determined with respect to the centre of the group:

$$V'_l = v_l - v_{l0}, \quad (16)$$

$$V'_b = v_b - v_{b0}, \quad (17)$$

in five OB-associations: Sgr OB1, Per OB1, Gem OB1, Car OB1 and Sco OB1, which demonstrate significant expansion in both cases: in the observed relative velocities and after their correction for the motion of the group as a whole. Four

**Table 2.** Average velocity dispersion inside OB-associations

| Row | Catalog         | Condition    | $\overline{\sigma_{vl}}$<br>(km s <sup>-1</sup> ) | $\overline{\sigma_{vb}}$<br>(km s <sup>-1</sup> ) | $\overline{\sigma_v}$<br>(km s <sup>-1</sup> ) | $n$ | Comments  |
|-----|-----------------|--------------|---|---|--|-----|---|
| 1   | <i>Gaia</i> DR2 | $n_\mu > 20$ | 4.96±0.49   | 3.96±0.36   | 4.46±0.30                                      | 28  | Stars identified with <i>Gaia</i> DR2               |
| 2   | <i>Gaia</i> DR2 | $n_\mu > 10$ | 4.65±0.39   | 4.69±0.33   | 4.17±0.26                                      | 40  | Stars identified with <i>Gaia</i> DR2               |
| 3   | <i>Gaia</i> DR2 | $n_\mu > 10$ | 4.69±0.49   | 3.96±0.47   | 4.33±0.34                                      | 23  | Common stars for <i>Gaia</i> DR2 and Hipparcos      |
| 4   | <i>Gaia</i> DR2 | $n_\mu > 10$ | 5.30±0.88   | 4.42±0.81   | 4.86±0.60                                      | 14  | Common stars for <i>Gaia</i> DR1, DR2 and Hipparcos |
| 5   | <i>Gaia</i> DR1 | $n_\mu > 10$ | 3.77±0.64   | 3.30±0.75   | 3.54±0.49                                      | 16  | Common stars for <i>Gaia</i> DR1 and Hipparcos      |

**Table 3.** Virial and stellar masses of OB-associations,  $M_{vir}$  and  $M_{st}$ , and star formation efficiency  $\epsilon$ 

| Name     | $l$<br>(deg) | $b$<br>(deg) | $r$<br>(kpc) | $V_r$<br>(km s <sup>-1</sup> ) | $\sigma_{vl}$<br>(km s <sup>-1</sup> ) | $\sigma_{vb}$<br>(km s <sup>-1</sup> ) | $a$<br>(kpc) | $n_\mu$ | $M_{vir}$<br>$M_\odot$ | $M_{st}$<br>$M_\odot$  | $N_{20}$ | $\epsilon$ 100%  |
|----------|--------------|--------------|--------------|--------------------------------|--|--|--------------|---------|------------------------|------------------------|----------|------------------|
| SGR OB5  | 0.04         | -1.16        | 2.42         | -15.0 ( 2)                     | 13.4                                   | 7.0                                    | 0.068        | 27      | 83.2 × 10 <sup>5</sup> | 7.5 × 10 <sup>3</sup>  | 18       | 0.1              |
| SGR OB1  | 7.54         | -0.77        | 1.26         | -10.0 (37)                     | 2.5                                    | 5.0                                    | 0.037        | 47      | 6.0 × 10 <sup>5</sup>  | 9.2 × 10 <sup>3</sup>  | 22       | 1.5              |
| SER OB1  | 16.71        | 0.07         | 1.53         | -5.0 (17)                      | 4.0                                    | 4.0                                    | 0.051        | 33      | 9.7 × 10 <sup>5</sup>  | 8.3 × 10 <sup>3</sup>  | 20       | 0.9              |
| CYG OB3  | 72.76        | 2.04         | 1.83         | -10.0 (29)                     | 6.8                                    | 4.1                                    | 0.024        | 32      | 8.5 × 10 <sup>5</sup>  | 10.8 × 10 <sup>3</sup> | 26       | 1.3              |
| CYG OB1  | 75.84        | 1.12         | 1.46         | -13.5 (34)                     | 6.2                                    | 3.6                                    | 0.032        | 62      | 9.0 × 10 <sup>5</sup>  | 16.7 × 10 <sup>3</sup> | 40       | 1.8              |
| CYG OB9  | 77.81        | 1.80         | 0.96         | -19.5 (10)                     | 3.4                                    | 3.4                                    | 0.017        | 22      | 2.3 × 10 <sup>5</sup>  | 4.6 × 10 <sup>3</sup>  | 11       | 2.0              |
| CYG OB8  | 77.92        | 3.36         | 1.83         | -21.0 ( 9)                     | 4.7                                    | 9.5                                    | 0.040        | 20      | 23.5 × 10 <sup>5</sup> | 6.7 × 10 <sup>3</sup>  | 16       | 0.3              |
| CYG OB7  | 88.98        | 0.03         | 0.63         | -9.4 (21)                      | 11.0                                   | 2.2                                    | 0.051        | 22      | 25.7 × 10 <sup>5</sup> | 2.9 × 10 <sup>3</sup>  | 7        | 0.1              |
| CEP OB2  | 102.02       | 4.69         | 0.73         | -17.0 (36)                     | 5.3                                    | 4.7                                    | 0.046        | 45      | 13.5 × 10 <sup>5</sup> | 7.9 × 10 <sup>3</sup>  | 19       | 0.6              |
| CAS OB2  | 111.99       | -0.00        | 2.10         | -50.1 ( 7)                     | 7.8                                    | 6.5                                    | 0.056        | 30      | 33.4 × 10 <sup>5</sup> | 9.6 × 10 <sup>3</sup>  | 23       | 0.3              |
| CAS OB5  | 116.09       | -0.50        | 2.01         | -45.8 (16)                     | 3.6                                    | 3.7                                    | 0.043        | 45      | 6.7 × 10 <sup>5</sup>  | 9.6 × 10 <sup>3</sup>  | 23       | 1.4              |
| CAS OB4  | 120.05       | -0.30        | 2.30         | -37.0 ( 7)                     | 7.8                                    | 5.3                                    | 0.070        | 24      | 34.9 × 10 <sup>5</sup> | 5.4 × 10 <sup>3</sup>  | 13       | 0.2              |
| CAS OB7  | 122.98       | 1.22         | 2.01         | -50.0 ( 4)                     | 3.7                                    | 2.4                                    | 0.041        | 35      | 4.6 × 10 <sup>5</sup>  | 6.7 × 10 <sup>3</sup>  | 16       | 1.5              |
| CAS OB8  | 129.16       | -1.06        | 2.30         | -34.6 (14)                     | 1.7                                    | 2.1                                    | 0.037        | 41      | 1.6 × 10 <sup>5</sup>  | 8.3 × 10 <sup>3</sup>  | 20       | 5.3              |
| PER OB1  | 134.70       | -3.14        | 1.83         | -43.2 (80)                     | 3.7                                    | 2.9                                    | 0.064        | 150     | 5.7 × 10 <sup>5</sup>  | 36.2 × 10 <sup>3</sup> | 87       | 6.4 <sup>a</sup> |
| CAS OB6  | 134.95       | 0.72         | 1.75         | -42.6 (12)                     | 4.6                                    | 5.9                                    | 0.057        | 29      | 18.5 × 10 <sup>5</sup> | 6.7 × 10 <sup>3</sup>  | 16       | 0.4              |
| CAM OB1  | 141.08       | 0.89         | 0.80         | -11.0 (30)                     | 3.3                                    | 2.9                                    | 0.079        | 41      | 8.8 × 10 <sup>5</sup>  | 5.0 × 10 <sup>3</sup>  | 12       | 0.6              |
| AUR OB1  | 173.83       | 0.14         | 1.06         | -1.9 (26)                      | 4.0                                    | 3.0                                    | 0.072        | 31      | 10.2 × 10 <sup>5</sup> | 3.7 × 10 <sup>3</sup>  | 9        | 0.4              |
| ORI OB1  | 206.90       | -17.71       | 0.40         | 25.4 (62)                      | 2.9                                    | 1.7                                    | 0.035        | 54      | 2.2 × 10 <sup>5</sup>  | 3.3 × 10 <sup>3</sup>  | 8        | 1.5              |
| GEM OB1  | 188.96       | 2.22         | 1.21         | 16.0 (18)                      | 3.8                                    | 2.5                                    | 0.042        | 35      | 4.8 × 10 <sup>5</sup>  | 5.4 × 10 <sup>3</sup>  | 13       | 1.1              |
| MON OB2  | 207.35       | -1.60        | 1.21         | 23.0 (25)                      | 3.3                                    | 4.0                                    | 0.037        | 23      | 5.6 × 10 <sup>5</sup>  | 5.4 × 10 <sup>3</sup>  | 13       | 1.0              |
| VELA OB1 | 264.83       | -1.41        | 1.46         | 23.0 (18)                      | 4.1                                    | 3.5                                    | 0.057        | 43      | 9.5 × 10 <sup>5</sup>  | 10.4 × 10 <sup>3</sup> | 25       | 1.1              |
| CAR OB1  | 286.45       | -0.46        | 2.01         | -5.0 (39)                      | 7.6                                    | 3.2                                    | 0.064        | 101     | 15.5 × 10 <sup>5</sup> | 20.8 × 10 <sup>3</sup> | 50       | 1.3 <sup>a</sup> |
| CAR OB2  | 290.39       | 0.12         | 1.83         | -8.2 (22)                      | 3.8                                    | 2.6                                    | 0.028        | 48      | 3.3 × 10 <sup>5</sup>  | 10.4 × 10 <sup>3</sup> | 25       | 3.1              |
| CRU OB1  | 294.87       | -1.06        | 2.01         | -5.3 (33)                      | 4.1                                    | 2.5                                    | 0.040        | 65      | 5.1 × 10 <sup>5</sup>  | 9.6 × 10 <sup>3</sup>  | 23       | 1.9              |
| CEN OB1  | 304.14       | 1.44         | 1.92         | -19.0 (32)                     | 5.1                                    | 2.9                                    | 0.068        | 85      | 12.5 × 10 <sup>5</sup> | 20.4 × 10 <sup>3</sup> | 49       | 1.6              |
| ARA OB1A | 337.68       | -0.92        | 1.10         | -36.3 ( 8)                     | 4.6                                    | 7.8                                    | 0.046        | 42      | 20.6 × 10 <sup>5</sup> | 4.6 × 10 <sup>3</sup>  | 11       | 0.2              |
| SCO OB1  | 343.72       | 1.37         | 1.53         | -28.8 (28)                     | 2.1                                    | 2.3                                    | 0.013        | 66      | 0.8 × 10 <sup>5</sup>  | 11.7 × 10 <sup>3</sup> | 28       | 15.0             |

Note.<sup>a</sup> Values of  $M_{vir}$  and  $\epsilon$  for the Per OB1 and Car OB1 associations are corrected for the expansion effect (Section 3.3)

other associations (Ori OB1, Cyg OB8, Cas OB2 and Mon OB2) will be discussed below.

Here we excluded from consideration 17 member stars with the absolute values of the relative velocities,  $V'_l$  or  $V'_b$ , greater than 50 km s<sup>-1</sup>, because such large velocities cannot be connected with expansion of OB-associations and are possibly due to binary systems or runaway stars (Fujii & Portegies Zwart 2011, see Appendix).

Figure 2 also indicates the positions of O-type stars, which are the youngest in OB-associations. We can see that O-type stars are distributed more or less uniformly among other stars of OB-associations.

Figure 2 shows that the Sgr OB1 association includes several groups of stars moving in opposite directions

along the  $X_b$ -axis. We do not observe here the expansion from one point as it is, for example, in the Per OB1 or Car OB1 association. The method of cluster analysis also shows that Sgr OB1 includes at least two different groups (Melnik & Efremov 1995).

As for Gem OB1, it is just the exclusion of five stars with the error RUWE > 1.4 from consideration that allows us to find the expansion inside this association.

Figure 3 shows the distribution of relative velocities in the Ori OB1 association: Figure 3(a) displays the observed relative velocities, whereas Figure 3(b) shows the velocities corrected for the motion of the association as a whole,  $V'_{lc}$  and  $V'_{bc}$ :

$$V'_{lc} = V'_l + V_r \frac{X_l}{r}, \quad (18)$$

$$V'_{bc} = V'_b + V_r \frac{X_b}{r}, \quad (19)$$

where the pair  $(X_l, X_b)$  are the coordinates of a star in the sky plane measured from the centre of OB-association along  $l$ - and  $b$ -direction, respectively. The velocity corrections are zero at the centre of the group and increase towards its periphery. The velocity of spurious expansion,  $e_1$  (Eq. 14), in the Ori OB1 association is quite large in absolute value,  $e_1 = -2.2 \text{ km s}^{-1}$  (Table 4), which is due to its location near the Sun ( $r = 0.4 \text{ kpc}$ ) and its large line-of-sight velocity,  $V_r = +25.4 \text{ km s}^{-1}$ , resulting from a combined contribution due to the solar motion to the apex ( $+13 \text{ km s}^{-1}$ ), the rotation curve ( $+5 \text{ km s}^{-1}$ ) and the residual velocity ( $+7 \text{ km s}^{-1}$ ). Note that the motion of the Ori OB1 association away from the Sun produces spurious compression. Figure 3 shows that after the correction for the spurious compression, the relative velocities demonstrate small expansion in the  $l$ -direction.

To check the expansion of the Ori OB1 association we analyze the distribution of relative velocities in the  $(X_l, X_r)$  plane, where the  $X_r$ -axis is directed along the line of sight connecting the Sun and the centre of the Ori OB1 association (Fig. 4). The coordinate  $X_r$  and the relative velocity  $V'_r$  of a star are derived from the *Gaia* DR2 parallax,  $\pi$ , and the stellar line-of-sight velocity,  $V_r$ , in the following way:

$$X_r = \frac{1}{\pi} \cos \phi - \frac{1}{\pi_0}, \quad (20)$$

$$V'_r = V_r \cos \phi - V_{r0}, \quad (21)$$

where  $\pi_0$  is the median parallax of stars of the Ori OB1 association;  $V_{r0}$  is the average stellar line-of-sight velocity projected onto the  $X_r$ -direction, and the angle  $\phi$  is the heliocentric angle between the direction to the star and to the centre of the association:

$$\phi = \arctan \frac{\sqrt{X_l^2 + X_b^2}}{r}, \quad (22)$$

which takes values in the range  $|\phi| < 13^\circ$ .

The parameter of expansion in the  $X_r$ -direction,  $p_r$ , is determined by solving the equations:

$$V'_r = p_r X_r. \quad (23)$$

Figure 4 shows conspicuous expansion of the Ori OB1 association along the line of sight. The parameter of expansion appears to be  $p_r = 105 \pm 29 \text{ km s}^{-1} \text{ kpc}^{-1}$  which corresponds to the specific velocity of expansion,  $u_r$ :

$$u_r = p_r a, \quad (24)$$

equal to  $u_r = 3.6 \pm 1.0 \text{ km s}^{-1}$ . Here we use the line-of-sight velocities,  $V_r$ , and parallaxes,  $\pi$ , measured with the uncertainties less than  $5 \text{ km s}^{-1}$  and  $0.2 \text{ mas}$ , respectively, which are available for 36 stars of the Ori OB1 association. The stellar line-of-sight velocities are taken from the catalog by Barbier-Brossat & Figon (2000).

We found that the expansion/compression in the Cyg OB8, Cas OB2 and Mon OB2 associations relies on the velocities of only a few stars. The exclusion of  $\sim 10$  per cent of stars with *Gaia* DR2 proper motions from these associations (HD 191423 and HD 191778 from Cyg OB8, BD+63

1964 from Cas OB2, HD 262042, HD 47732 and HD 47777 from Mon OB2) decreases the absolute value of expanding/compressing velocity,  $\tilde{u}_l$  or  $\tilde{u}_b$ , down to a significance level of less than  $2\sigma$ .

Figure 5 shows the dependence of the stellar proper motions,  $\mu_l$  and  $\mu_b$ , on the coordinates  $l$  and  $b$ , respectively, for the associations Sgr OB1, Gem OB1, Ori OB1, Per OB1, Car OB1 and Sco OB1. Also shown is the expected dependence due to the motion of the association as a whole. We can see that in all cases except Ori OB1, the correlation between  $\mu_l$  and  $l$  or between  $\mu_b$  and  $b$  is positive and greater than the correlation due to spurious expansion. Positive correlation between the coordinate and corresponding proper motion suggests expansion, whereas negative correlation means compression. The Ori OB1 association is a special case – here one expects to see considerable negative correlation between  $\mu_l$  and  $l$  (the dashed line) caused by the motion of the association away from the Sun with  $V_r = 25 \text{ km s}^{-1}$ , but the observed dependence (the red line) is much weaker than the expected one, which indicates the presence of some physical expansion practically compensating its spurious compression.

### 3.4 Kinematic ages of OB-associations

We can make crude estimates of stellar ages on the basis of their spectral types (effective temperatures) and luminosities using available stellar models and various photometric calibrations. The ages of O8 stars of all luminosity classes must be smaller than 5 Myr, while B0 stars must be younger than 10 Myr (Bressan et al. 2012). So the ages of OB-associations are supposed to be 5–10 Myr. However, the low-mass stars born in the same molecular cloud can be conspicuously older, some estimates of their ages are as old as 20–50 Myr (Pecaut & Mamajek 2016; Cantat-Gaudin et al. 2019). In this context it is interesting to compare the ages of OB-associations derived from stellar models (the so-called stellar ages) with their kinematic ages, i.e. the time instants in the past when the group had minimal size. There are two classical methods of the determination of kinematic ages. One method derives the kinematic ages from  $p_l$  and  $p_b$ , while another is based of the backtracing the positions of individual stars. Brown, Dekker & de Zeeuw (1997) tested both methods and found that the first method overestimates the kinematic age while the second method, on the contrary, underestimates it.

Table 5 presents the estimates of the kinematic ages determined by two different ways. The values  $T_l$  and  $T_b$  are computed by the first method through the values of  $p_l$ ,  $p_b$ ,  $e_1$  and  $a$ :

$$T_l = [(p_l - \frac{e_1}{a}) f_v]^{-1}, \quad (25)$$

$$T_b = [(p_b - \frac{e_1}{a}) f_v]^{-1}, \quad (26)$$

where factor  $f_v = 1.023 \cdot 10^{-3}$  transforms velocities in units of  $\text{km s}^{-1}$  into  $\text{kpc Myr}^{-1}$ . The parameters of expansion,  $p_l$  and  $p_b$ , were corrected for the motion of the association as a whole.

The second method is based on the positions and proper motions of individual stars. We determine the positions of member stars in the past using their present-day coordinates

**Table 4.** Expansion/compression of OB-associations with *Gaia* DR2 proper motions

| Name     | $p_l$<br>(km s <sup>-1</sup> kpc <sup>-1</sup> ) | $p_b$<br>(km s <sup>-1</sup> kpc <sup>-1</sup> ) | $a$<br>(kpc) | $u_l$<br>(km s <sup>-1</sup> ) | $u_b$<br>(km s <sup>-1</sup> ) | $e_1$<br>(km s <sup>-1</sup> ) | $\tilde{u}_l$<br>(km s <sup>-1</sup> ) | $\tilde{u}_b$<br>(km s <sup>-1</sup> ) | $n_\mu$ |
|----------|--|--|--------------|--------------------------------|--------------------------------|--------------------------------|--|--|---------|
| SGR OB5  | 64 ± 63  | -4 ± 25  | 0.068        | 4.4 ± 4.3                      | -0.3 ± 1.7                     | 0.43 ± 0.10                    | 4.0 ± 4.3                              | -0.7 ± 1.7                             | 27      |
| SGR OB1  | -13 ± 11   | 145 ± 36   | 0.037        | -0.5 ± 0.4                     | 5.3 ± 1.3                      | 0.29 ± 0.05                    | -0.8 ± 0.4                             | <u>5.0 ± 1.3</u>                       | 47      |
| SER OB1  | -1 ± 33  | 44 ± 41  | 0.051        | -0.1 ± 1.7                     | 2.2 ± 2.1                      | 0.17 ± 0.12                    | -0.2 ± 1.7                             | <u>2.1 ± 2.1</u>                       | 33      |
| CYG OB3  | 249 ± 109  | 139 ± 67   | 0.024        | 6.1 ± 2.6                      | 3.4 ± 1.6                      | 0.13 ± 0.02                    | 5.9 ± 2.6                              | <u>3.3 ± 1.6</u>                       | 31      |
| CYG OB1  | -5 ± 68  | 25 ± 35  | 0.032        | -0.2 ± 2.2                     | 0.8 ± 1.1                      | 0.30 ± 0.02                    | -0.5 ± 2.2                             | <u>0.5 ± 1.1</u>                       | 62      |
| CYG OB9  | 162 ± 85   | 113 ± 176  | 0.017        | 2.8 ± 1.5                      | 2.0 ± 3.0                      | 0.35 ± 0.03                    | 2.5 ± 1.5                              | <u>1.6 ± 3.0</u>                       | 22      |
| CYG OB8  | -46 ± 93   | 178 ± 47   | 0.040        | -1.8 ± 3.7                     | 7.1 ± 1.9                      | 0.46 ± 0.05                    | -2.3 ± 3.7                             | <u>6.7 ± 1.9</u>                       | 19      |
| CYG OB7  | -67 ± 69   | 122 ± 51   | 0.051        | -3.4 ± 3.5                     | 6.2 ± 2.6                      | 0.76 ± 0.16                    | -4.1 ± 3.5                             | <u>5.4 ± 2.6</u>                       | 22      |
| CEP OB2  | 72 ± 27  | 14 ± 22  | 0.046        | 3.4 ± 1.2                      | 0.6 ± 1.0                      | 1.09 ± 0.06                    | 2.3 ± 1.2                              | -0.4 ± 1.0                             | 45      |
| CAS OB2  | -32 ± 58   | 121 ± 33   | 0.056        | -1.8 ± 3.2                     | 6.8 ± 1.8                      | 1.34 ± 0.05                    | -3.1 ± 3.2                             | <u>5.4 ± 1.8</u>                       | 29      |
| CAS OB5  | 54 ± 32  | 49 ± 22  | 0.043        | 2.3 ± 1.4                      | 2.1 ± 1.0                      | 0.99 ± 0.02                    | 1.3 ± 1.4                              | <u>1.1 ± 1.0</u>                       | 45      |
| CAS OB4  | 95 ± 55  | 63 ± 20  | 0.070        | 6.7 ± 3.8                      | 4.4 ± 1.4                      | 1.13 ± 0.05                    | 5.6 ± 3.8                              | <u>3.3 ± 1.4</u>                       | 22      |
| CAS OB7  | 74 ± 27  | 63 ± 35  | 0.041        | 3.0 ± 1.1                      | 2.6 ± 1.4                      | 1.02 ± 0.00                    | 2.0 ± 1.1                              | <u>1.6 ± 1.4</u>                       | 34      |
| CAS OB8  | 51 ± 17  | 37 ± 19  | 0.037        | 1.9 ± 0.6                      | 1.4 ± 0.7                      | 0.56 ± 0.02                    | 1.3 ± 0.6                              | <u>0.8 ± 0.7</u>                       | 40      |
| PER OB1  | 51 ± 9   | 65 ± 10  | 0.064        | 3.3 ± 0.6                      | 4.2 ± 0.6                      | 1.52 ± 0.02                    | <u>1.8 ± 0.6</u>                       | <u>2.7 ± 0.6</u>                       | 149     |
| CAS OB6  | 89 ± 30  | 185 ± 39   | 0.057        | 5.1 ± 1.7                      | 10.6 ± 2.2                     | 1.39 ± 0.05                    | <u>3.7 ± 1.7</u>                       | <u>9.2 ± 2.2</u>                       | 28      |
| CAM OB1  | 36 ± 14  | -21 ± 17   | 0.079        | 2.8 ± 1.1                      | -1.6 ± 1.3                     | 1.08 ± 0.14                    | 1.7 ± 1.1                              | -2.7 ± 1.3                             | 41      |
| AUR OB1  | 11 ± 14  | -8 ± 15  | 0.072        | 0.8 ± 1.0                      | -0.6 ± 1.1                     | 0.13 ± 0.17                    | 0.7 ± 1.0                              | -0.7 ± 1.1                             | 31      |
| ORI OB1  | -15 ± 14   | -57 ± 16   | 0.035        | -0.5 ± 0.5                     | -2.0 ± 0.5                     | -2.21 ± 0.09                   | <u>1.7 ± 0.5</u>                       | 0.2 ± 0.5                              | 54      |
| GEM OB1  | 10 ± 34  | 77 ± 26  | 0.042        | 0.4 ± 1.4                      | 3.2 ± 1.1                      | -0.55 ± 0.03                   | 1.0 ± 1.4                              | <u>3.8 ± 1.1</u>                       | 35      |
| MON OB2  | -215 ± 45  | 36 ± 66  | 0.037        | -7.9 ± 1.6                     | 1.3 ± 2.4                      | -0.70 ± 0.07                   | <u>-7.2 ± 1.6</u>                      | 2.0 ± 2.4                              | 23      |
| VELA OB1 | 26 ± 22  | -29 ± 16   | 0.057        | 1.5 ± 1.2                      | -1.7 ± 0.9                     | -0.89 ± 0.03                   | 2.4 ± 1.2                              | -0.8 ± 0.9                             | 42      |
| CAR OB1  | 101 ± 14   | 37 ± 14  | 0.064        | 6.5 ± 0.9                      | 2.4 ± 0.9                      | 0.16 ± 0.03                    | <u>6.3 ± 0.9</u>                       | 2.2 ± 0.9                              | 100     |
| CAR OB2  | 59 ± 59  | 83 ± 27  | 0.028        | 1.6 ± 1.6                      | 2.3 ± 0.8                      | 0.13 ± 0.02                    | <u>1.5 ± 1.6</u>                       | 2.2 ± 0.8                              | 48      |
| CRU OB1  | 35 ± 31  | 33 ± 16  | 0.040        | 1.4 ± 1.2                      | 1.3 ± 0.6                      | 0.11 ± 0.02                    | 1.3 ± 1.2                              | 1.2 ± 0.6                              | 64      |
| CEN OB1  | -18 ± 18   | 13 ± 11  | 0.068        | -1.2 ± 1.2                     | 0.9 ± 0.7                      | 0.67 ± 0.06                    | -1.9 ± 1.2                             | 0.2 ± 0.7                              | 84      |
| ARA OB1A | 31 ± 31  | 82 ± 39  | 0.046        | 1.4 ± 1.4                      | 3.7 ± 1.8                      | 1.51 ± 0.13                    | -0.1 ± 1.4                             | 2.2 ± 1.8                              | 42      |
| SCO OB1  | 224 ± 29   | 142 ± 38   | 0.013        | 3.0 ± 0.4                      | 1.9 ± 0.5                      | 0.25 ± 0.02                    | <u>2.8 ± 0.4</u>                       | <u>1.7 ± 0.5</u>                       | 66      |

and velocities. Here we suppose that stars in an association start their expansion at one moment in the past but with different velocities. The observed velocities computed with respect to the centre of the association,  $v'_l$  and  $v'_b$ , were corrected for the motion of the association as a whole:

$$x(t) = x_0 - (v'_l + V_r \frac{x_0}{r})t, \quad (27)$$

$$y(t) = y_0 - (v'_b + V_r \frac{y_0}{r})t, \quad (28)$$

The selection of the most compact part of association allows us to mitigate changes due to inclusion or exclusion of individual stars. Only cases with well-defined expansion are considered.

Figure 6 shows the dependence of the size of OB-association,  $s$ , on the time  $t$  in the past. The value  $s$  is the radius of the association containing central 68 per cent of its members with known *Gaia* proper motions. Note that the second method is very sensitive to the errors in proper motions of individual stars. So we select stars with the most precise proper motions in the Per OB1 association and calculate function  $s(t)$  for this sample as well. The new sample includes stars with  $\varepsilon_{\mu l} < 0.008$  mas yr<sup>-1</sup> and  $\varepsilon_{\mu b} < 0.008$  mas yr<sup>-1</sup> leaving 38 stars in the Per OB1 association.

Figure 6 shows that function  $s(t)$  has a minimum in some cases and a plateau with subsequent growth in others. In the Per OB1 association the sample of stars with the most precise proper motions shows minimum on the curve  $s(t)$  while the sample including all stars with *Gaia* DR2 proper

motions gives a plateau. The selection of stars with the most accurate proper motions does not change the results in the Sgr OB1, Car OB1 and Sco OB1 associations, so we don't demonstrate them separately. Note that the average uncertainty in determination of *Gaia* DR2 proper motions in the Ori OB1 association is  $\varepsilon_{\mu l} = 0.230$  mas yr<sup>-1</sup>, and the criteria considered leaves no stars here.

Kinematic ages of OB-associations obtained by the second method,  $T^*$ , correspond to the minimum on the curves  $s(t)$ . Note that a considerable difference between the minimum and present-day sizes of an association:

$$\xi = s(T_i^*)/s(0), \quad (29)$$

is observed only in the Per OB1 and Car OB1 associations equal to  $\xi = 0.69$  and  $\xi = 0.73$ , respectively. The minimal radii of OB-associations corresponding to the plateau or to a minimum of functions  $s(t)$  are: 67 pc (Per OB1), 47 pc (Car OB1), 10 pc (Sco OB1), 35 pc (Sgr OB1), 29 pc (Ori OB1). These values are located in the interval 10–100 pc corresponding to the expected sizes of giant molecular clouds (Sanders, Scoville & Solomon 1985).

Table 5 lists the kinematic ages  $T^*$  and their errors calculated from the uncertainties in proper motions which cause the uncertainties in the determination of sizes of OB-associations,  $\Delta s$ , proportional to the time interval in the past:

$$\Delta s = 4.74 r \varepsilon_\mu T^* f_v, \quad (30)$$

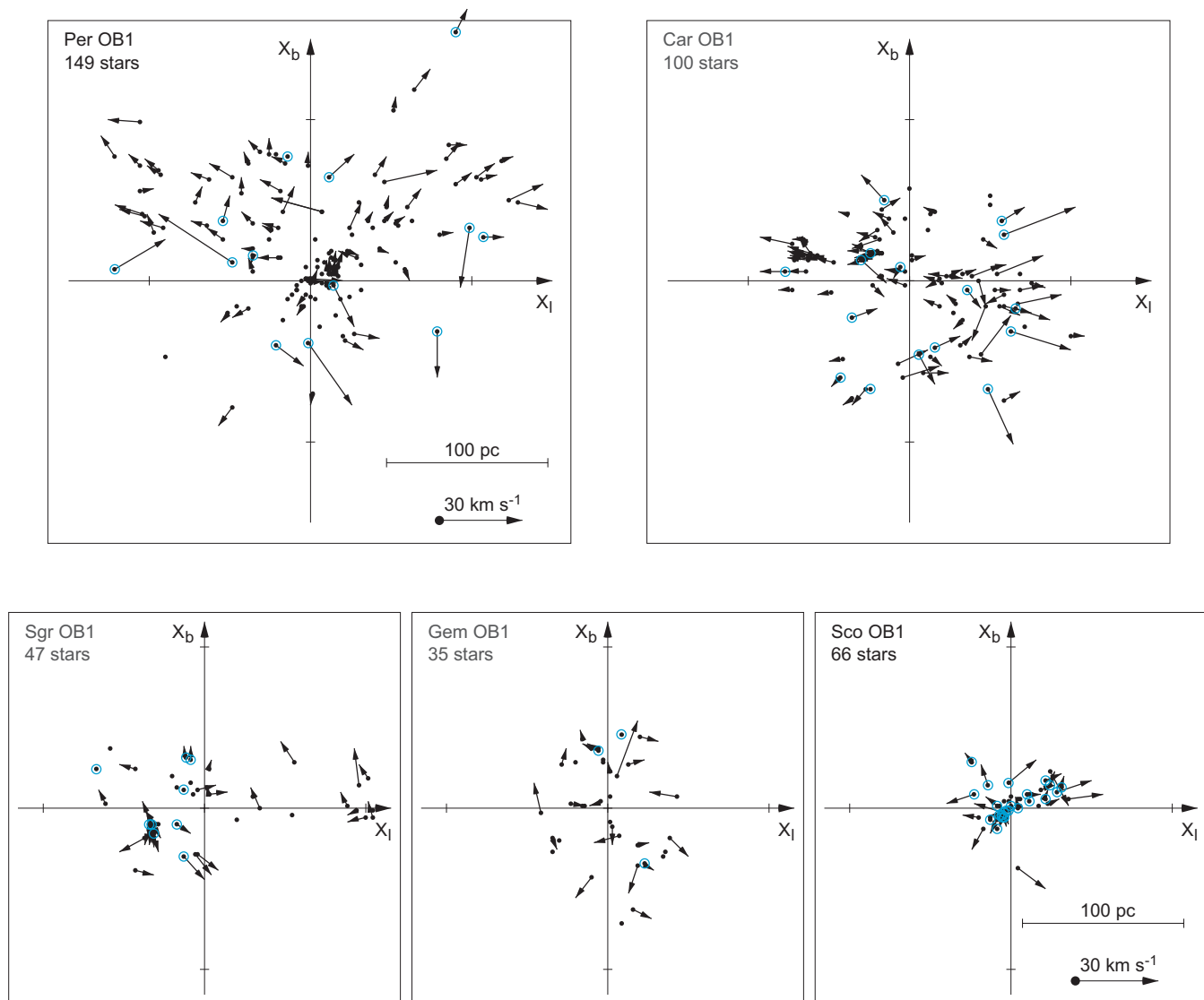


**Figure 2.** Distribution of observed relative velocities,  $V'_l$  and  $V'_b$ , in the Per OB1, Car OB1, Sgr OB1, Gem OB1 and Sco OB1 associations. All frames have the same scale. The velocities  $V'_l$  and  $V'_b$  are determined with respect to the centre of the association (Eqs 16 and 17). Stars with the relative velocities  $|V'_l|$  and  $|V'_b|$  smaller than  $3 \text{ km s}^{-1}$  are shown as black circles without any vector. The axes  $X_l$  and  $X_b$  are directed towards increasing values of Galactic coordinates,  $l$  and  $b$ , respectively. We can see conspicuous expansion in these associations. Stars of spectral type O are outlined by circles (colored blue in online article). O-type stars can be seen to be distributed more or less uniformly among other stars of OB-associations.

where  $\varepsilon_\mu$  is the average uncertainty in determination of proper motions in  $l$ - and  $b$ -directions. The values of  $\Delta s$  are as follows: 4 pc (Per OB1, sample of stars with the most precise proper motions), 2 pc (Car OB1, Sco OB1, Gem OB1), 1 pc (Sgr OB1, Ori OB1).

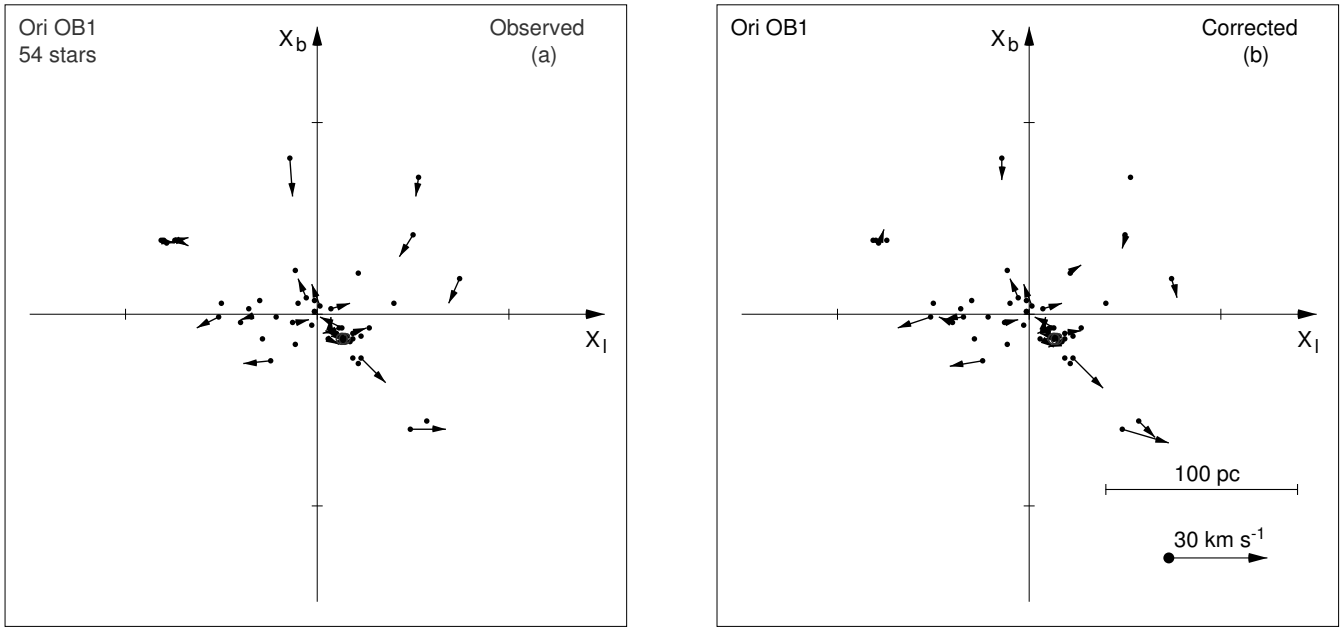
In the case of Sgr OB1 we can give only upper limit for the value of  $T^*$ . The values of  $T^*$  do not exceed 4 Myr except the case of the Per OB1 association where it amounts to  $T^* = 10.6^{+2.6}_{-3.9}$  Myr.

Table 5 suggests that the kinematic ages,  $T_l$  and  $T_b$ , obtained by the first method are always greater than corresponding estimates derived using the second method,  $T^*$ , which agrees with the results by Brown, Dekker & de Zeeuw (1997). The first method (Eqs. 25 and 26) is less sensitive to the errors in proper motions of individual stars: several erroneous proper motions cannot spoil the picture of overall

expansion (Fig. 5), but this method assumes that the OB-association expands from a point or from a very small region which can be incorrect in some cases. The second method (Eqs. 27 and 28) is more direct: it does not involve additional assumptions about the initial size of the group, but it is more sensitive to the errors in proper motions of individual stars which can completely wash out the expansion (Fig. 6).

Our estimates of the kinematic ages of OB-associations,  $T^*$ , obtained by the second method are smaller than 5 Myr in the Sgr OB1, Gem OB1, Ori OB1, Car OB1 and Sco OB1 associations which agrees with the following star-formation scenario: first OB-stars form inside a giant molecular cloud and only then a group of these stars starts its expansion. In the case of the Per OB1, the value of  $T^* = 10.6^{+2.6}_{-3.9}$  is only marginally consistent with this sequence of events. Possibly,





**Figure 3.** Distribution of observed,  $V'_l$  and  $V'_b$ , and corrected,  $V'_{lc}$  and  $V'_{bc}$  (Eqs 18 and 19), relative velocities in the Ori OB1 association. Stars with the relative velocities  $|V'_l|$  and  $|V'_b|$  smaller than  $3 \text{ km s}^{-1}$  are shown as black circles without any vector. The axes  $X_l$  and  $X_b$  point in the  $l$ - and  $b$ -direction, respectively. We can see small expansion along the  $X_l$ -axis in the distribution of relative velocities corrected for the motion of the association as a whole.

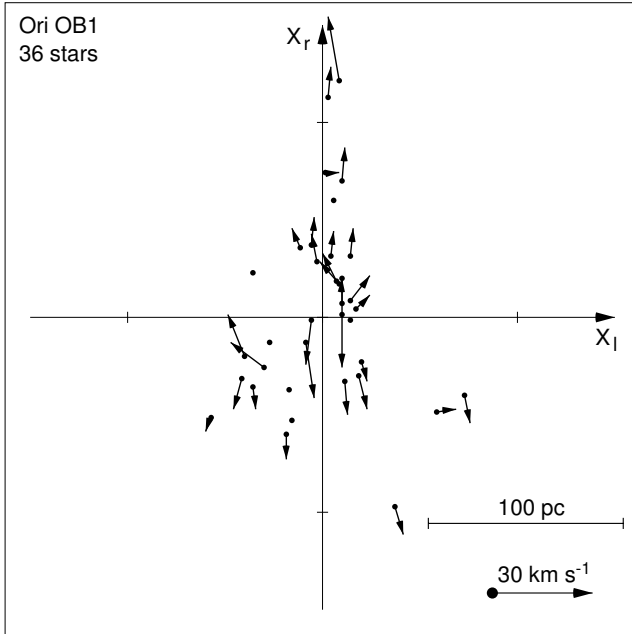


**Figure 4.** Distribution of relative velocities,  $V'_{lc}$  and  $V'_r$ , in the plane  $(X_l, X_r)$ , where the axes  $X_l$  and  $X_r$  point in the  $l$ -direction and along the line of sight connecting the Sun and the centre of the Ori OB1 association, respectively. The Sun is at the bottom. The velocity  $V'_r$  is the relative velocity along the line of sight (Eq. 21). The velocity  $V'_{lc}$  is the relative velocity in the  $l$ -direction corrected for the motion of the association as a whole (Eq. 18). Stars with the relative velocities  $|V'_{lc}|$  and  $|V'_r|$  smaller than  $3 \text{ km s}^{-1}$  are shown as black circles without any vector. We can see conspicuous expansion of the Ori OB1 association along the line of sight here.

**Table 5.** Kinematic ages of OB-associations

| Name    | $T_l$<br>Myr         | $T_b$<br>Myr        | $T^*$<br>Myr         |
|---------|----------------------|---------------------|----------------------|
| Sgr OB1 | –                    | $7.1^{+0.6}_{-1.5}$ | $< 1$                |
| Per OB1 | $36^{+17}_{-8}$      | $24^{+7}_{-5}$      | $10.6^{+2.6}_{-3.9}$ |
| Ori OB1 | $20.4^{+7.2}_{-4.6}$ | –                   | $2.7 \pm 0.3$        |
| Gem OB1 | $10.9^{+1.4}_{-2.4}$ | –                   | $2.5^{+0.1}_{-0.6}$  |
| Car OB1 | $9.9^{+1.6}_{-1.2}$  | –                   | $3.4^{+0.6}_{-0.8}$  |
| Sco OB1 | $4.8^{+0.8}_{-0.6}$  | $8.0^{+2.5}_{-1.9}$ | $2.1 \pm 1.4$        |

the Per OB1 association started its expansion with a larger velocity than its present-day value, resulting in a smaller kinematic age (see also section 3.5).

### 3.5 Shell-like structure in the distribution of stars in the Per OB1 association

The distribution of stars in two large expanding OB-associations, Per OB1 and Car OB1, suggests the presence of a shell-like structure with a density maximum located between the central part and periphery (Fig. 2). To check this hypothesis we consider the variations of the surface density of OB-stars,  $\Sigma$ , with the distance,  $d$ , from the centre of the association (Fig. 7a). We subdivided the distribution of stars in the sky-plane inside the association into 6 pc-wide annuli of radius  $d$  with the centres coincident with the centre of the association. The average surface density of stars at the

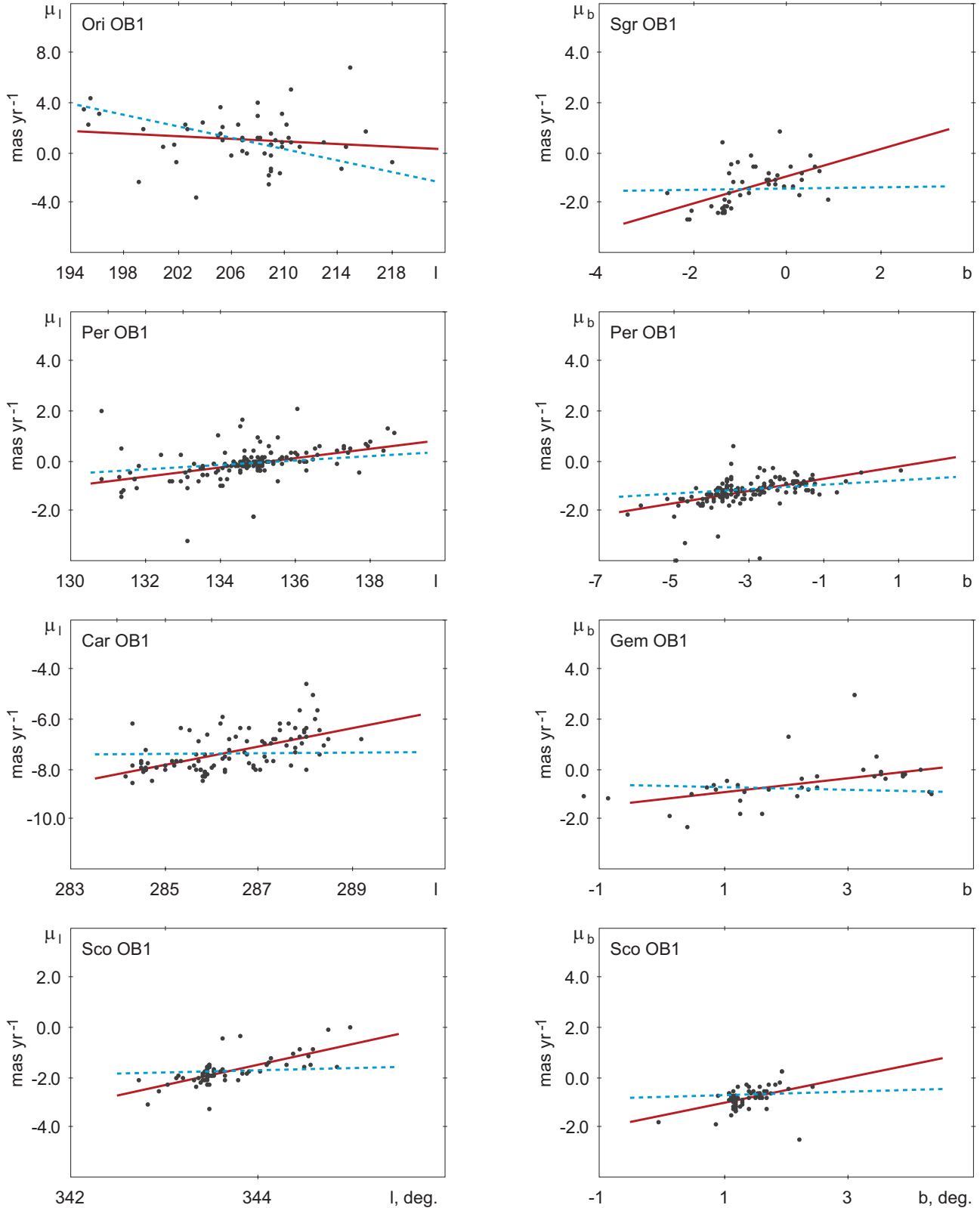


**Figure 5.** Dependence of stellar proper-motion components,  $\mu_l$  and  $\mu_b$ , on the corresponding coordinates,  $l$  and  $b$ , in the associations Sgr OB1, Per OB1, Ori OB1, Gem OB1, Car OB1 and Sco OB1. The solid lines (colored red in the online article) indicate the linear fits of the dependencies  $\mu_l(l)$  and  $\mu_b(b)$  determined from observational data while the dashed lines (colored blue in the online article) show the correlation between  $\mu_l$  and  $l$  or between  $\mu_b$  and  $b$ , which appears due to the motion of the association as a whole (Eq. 14). Positive correlation between the proper motion and corresponding coordinate means expansion while negative correlation indicates compression. In the Ori OB1 association, the spurious compression due to its motion along the line of sight is considerably larger than that derived from the observed data, which suggests the presence of a physical expansion.

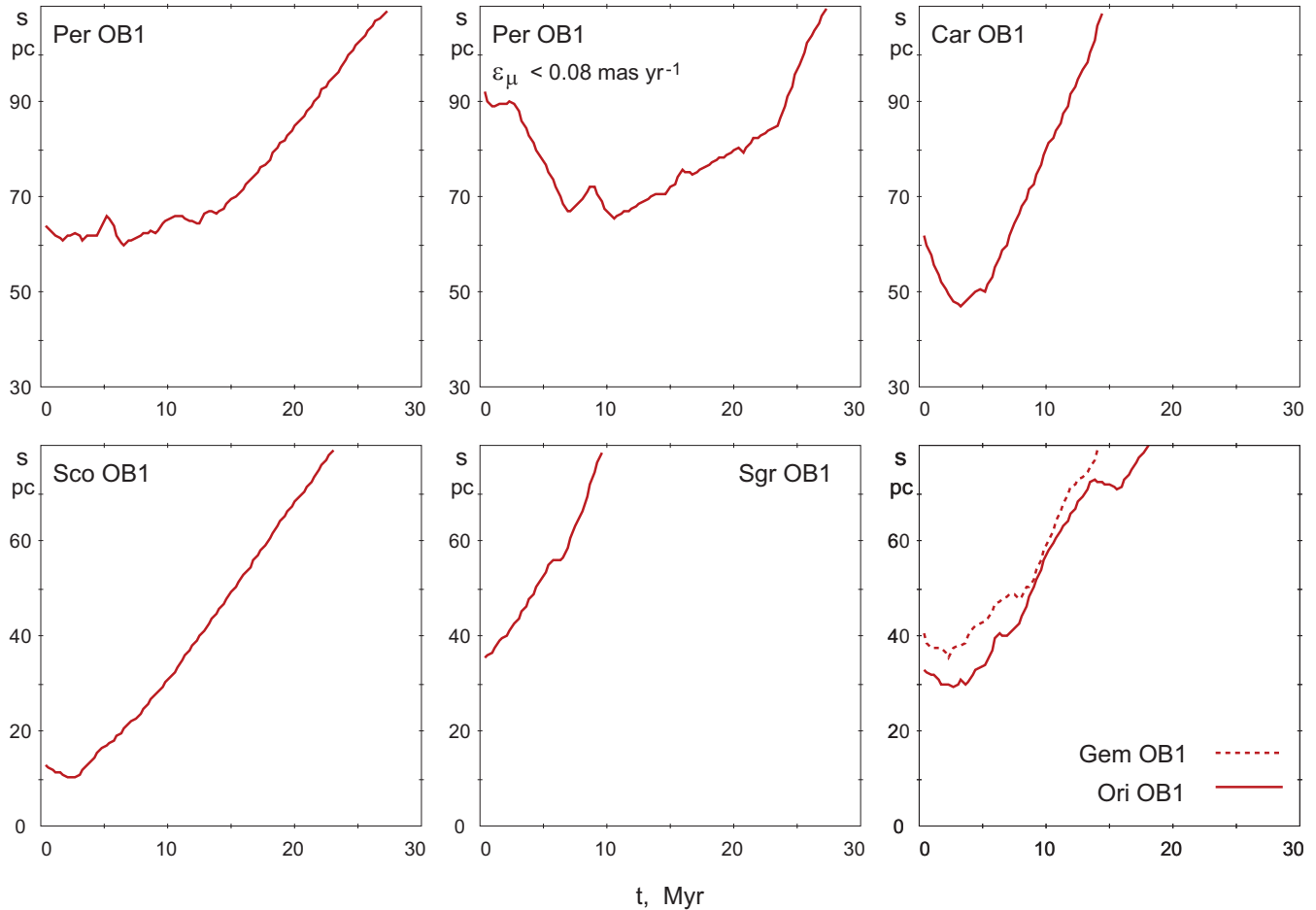


**Figure 6.** Dependence of the size  $s$  of OB-association on the time  $t$  in the past. Here  $s$  is the radius of association containing central 68 per cent of its star-members with known Gaia DR2 proper motions. In the case of the Per OB1 association we also show separate plot for the sample of stars with the most precise proper motions ( $\varepsilon_{\mu l} < 0.008 \text{ mas yr}^{-1}$  and  $\varepsilon_{\mu b} < 0.008 \text{ mas yr}^{-1}$ ). Only cases with well-defined parameters of expansion are considered.

distance  $d$  from the centre is the ratio  $\Sigma = N/S$ , where  $N$  is the number of stars in the annulus and  $S$  is its area.

Figure 7(a) shows the presence of a secondary maximum on the curve  $\Sigma(d)$  for the Per OB1 association located at the distance of 40 pc from its centre. The secondary maximum is due to the presence of a minimum on the density curve between the central concentration and the periphery. The statistical significance of the secondary maximum is determined by the errors due to Poisson noise in the maximum and minimum density distribution,  $\sigma_1$  and  $\sigma_2$ , respectively:

$$S = \frac{\Sigma_{max} - \Sigma_{min}}{\sigma_1 + \sigma_2}, \quad (31)$$

which gives the significance level of  $P \sim 1.4\sigma$ . We find a similar shell-like structure in the Car OB1 association but it has lower statistical significance and we do not consider it here.

To understand the nature of the secondary maximum we build the distribution of velocities inside the association. Figure 7(b) shows the variation of the average expansion velocity,  $V_{dc}$ , of OB-stars with the distance,  $d$ , from the centre of the association. The velocity  $V_{dc}$  of a star is the component of its relative corrected velocity,  $(V'_{lc}, V'_{bc})$  (Eqs. 18 and 19), directed along the radius-vector,  $\vec{d}$ , connecting

the centre of the association with the star in the sky plane. We can see that the velocity  $V_{dc}$  at the distance of the shell,  $d = 40 \text{ pc}$ , amounts to the value of  $V_{dc} = 5.0 \pm 1.7 \text{ km s}^{-1}$ . Thus, we can speak about the expanding shell of stars here.

There are two different scenarios of the formation of expanding OB-associations. The first one considers the expansion of young stellar group caused by the gas loss in its parent molecular cloud (Hills 1980; Kroupa, Aarseth & Hurley 2001; Boily & Kroupa 2003a,b; Vine & Bonnell 2003). The second scenario includes two episodes of star formation: the first generation of massive stars creates an expanding gas shell while the second generation of stars, which we observe now, forms from the molecular gas collected by the expanding shell. The radii of the shells are supposed to be 30–150 pc and the velocity of expansion  $V_{sh}$  must be less than  $V_{sh} < 15 \text{ km s}^{-1}$  (Castor, McCray & Weaver 1975; Weaver et al. 1977; Elmegreen & Lada 1977; Lozinskaya & Sitnik 1988; Lozinskaya 1999, and others). There is a difference between the formation of OB-stars in an expanding shell, when stars acquire the expansion velocity at the time of their birth, and the expansion of OB-association due to the gas loss in the parent molecular cloud, when stars are born in the turbulent but unexpanding gas medium and begin their motion

outwards due to a sudden lack of gravitational force in the centre of the group.

The formation of the Per OB1 association from the molecular gas accumulated by the shell seems to be unlikely. There are two arguments against this scenario. First, we do not observe any difference in ages of OB-stars located in the central part and in the expanding shell in the Per OB1 association (Fig. 2). Second, the symmetry in the distribution of stars with respect to the centre of the association. If stars were born in an expanding shell then they would have been formed in gravitationally isolated segments of the shell which must have a bit different density, so the formation of massive stars throughout the shell in a small time interval looks questionable.

We suppose that the expansion of the Per OB1 association is caused by the gas loss in its parent molecular cloud due to thermal pressure of HII regions. The average radius and expansion velocity of the shell are  $d = 40$  pc and  $V_{dc} = 5.0 \pm 1.7$  km s<sup>-1</sup>, respectively. It means that the Per OB1 association started its expansion  $T = 8_{-2}^{+4}$  Myr ago. However, the existence of massive O-type stars in the expanding shell, whose ages do not exceed 5 Myr (Fig. 2), suggests that the expansion of the Per OB1 association must have started with a larger expanding velocity and its kinematical age must be smaller than 5 Myr.

Note that the age of the double stellar cluster  $h$  and  $\chi$  Persei located in the centre of the Per OB1 association is supposed to be 10–13 Myr (Slesnick, Hillenbrand & Massey 2002; Dias et al. 2002), which suggests that the formation of their stars could have started 5–8 Myr before the formation of present-day O-stars in the Per OB1 association. Probably, stars of the clusters  $h$  and  $\chi$  Persei formed during the time interval when the parent molecular cloud was compressing due to its own gravity but the mean gas density had not reached its maximal value yet. Simulations show that during the global collapse of the cloud the average Jeans mass is decreasing and the fraction of gas mass involved in the instantaneous star formation is increasing, so the initial mass function is expected to be sufficiently sampled to produce massive stars which then begin to erode the cloud (Colin, Vazquez-Semadeni & Gomez 2013; Zamora-Aviles, Vazquez-Semadeni & Colin 2012). Probably, the giant molecular cloud in which the Per OB1 association formed had very dense central part which allowed it to produce a lot of massive stars during a small time interval.

#### 4 DISCUSSION AND CONCLUSIONS

We studied the velocities in the sky plane,  $v_l$  and  $v_b$ , inside 28 OB-associations including more than 20 *Gaia* DR2 stars. The average velocity dispersion inside 28 associations is  $\overline{\sigma}_v = 4.5 \pm 0.3$  km s<sup>-1</sup>, which exceeds the corresponding value derived from *Gaia* DR1 proper motions,  $\overline{\sigma}_v = 3.5 \pm 0.5$  km s<sup>-1</sup>, at the significance level of  $P \sim 1\sigma$ . The greater value of  $\sigma_v$  obtained with *Gaia* DR2 proper motions can be both due to statistical effects and due to shorter time base-line, which makes the results more sensitive to all sorts of systematic effects.

Kounkel et al. (2018) found that the line-of-sight velocities of stars inside the Ori OB1 association obtained with the uncertainty less than 1 km s<sup>-1</sup> and corrected for the

motion of the Sun toward the standard apex lie in the range 0–15 km s<sup>-1</sup> which is consistent with the velocity dispersion 3–5 km s<sup>-1</sup>.

We used the velocity dispersion  $\sigma_v$  inside OB-associations and their radii  $a$  to calculate the virial masses of OB-associations, which are equal to the masses of their parent giant molecular clouds. The median virial mass computed for 28 OB-associations is  $M_{vir} = 8.9 \times 10^5 M_\odot$ . We also determined the stellar masses of OB-associations. Here we used the power-law distribution of stars over masses by Kroupa (2002) calibrated through the number of massive stars in OB-association. The median stellar mass of OB-associations is  $M_{st} = 8.1 \times 10^3 M_\odot$ . The stellar to virial mass ratio determines the average star-formation efficiency inside the giant molecular cloud, which has the median value of  $\epsilon = 1.2$  per cent.

We found that the Sgr OB1, Per OB1, Ori OB1, Gem OB1, Car OB1 and Sco OB1 associations are expanding at a significance level of  $P > 3\sigma$ . The expansion of the Per OB1, Car OB1 and Sgr OB1 associations first have been found with *Gaia* DR1 proper motions (Melnik & Dambis 2017). *Gaia* DR2 data confirm their expansion and suggest three new expanding associations: Ori OB1, Gem OB1 and Sco OB1. The Ori OB1 association shows expansion only after the correction of velocities  $v_l$  and  $v_b$  for the line-of-sight motion of the association as a whole, it also displays the expansion along the line of sight. The expansion of the Gem OB1 association was found only after the exclusion of five stars with the error  $\text{RUWE} > 1.4$  from consideration. Only two associations (Per OB1 and Sco OB1) show well-defined expansion in both the  $l$ - and  $b$ -direction, the other associations demonstrate expansion at a significance level  $P > 3\sigma$  in one direction only.

We gave evidence in favour of the expanding stellar shell in the Per OB1 association with the radius of  $d = 40$  pc and the expansion velocity of  $V_{dc} = 5.0 \pm 1.7$  km s<sup>-1</sup>, which suggests that the expansion of OB-stars started  $T = 8_{-2}^{+4}$  Myr ago. However, the existence of massive O-type stars in the expanding shell with the ages less than 5 Myr suggests that the expansion of the Per OB1 association started with a larger expanding velocity, resulting in a smaller kinematic age.

We can see that the expansion of OB-associations is quite a rare event: it is observed only in 6 from 28 associations considered, i.e. the frequency of this event is  $\sim 21$  per cent. There are two possible reasons of such a low frequency of expanding OB-associations. First, it is the lack of precise proper motions for stars of OB-associations so the expansion is merely washed out by noise. Second, it is a physical reason – only the most dense giant molecular clouds can produce stellar groups expanding from one centre, while less dense clouds produce several groups inside one cloud each of which is expanding from its centre, so the total velocity distribution looks chaotic.

We found a strong correlation between the re-normalised unit weight errors (RUWE) and the relative velocities (Eqs 16 and 17) of member stars determined with respect to the centre of OB-association. Note that among 33 stars moving with the relative velocities more than 50 km s<sup>-1</sup> the fraction of stars with  $\text{RUWE} > 1.4$  amounts to 48 per cent but the expected fraction is only 9 per cent.

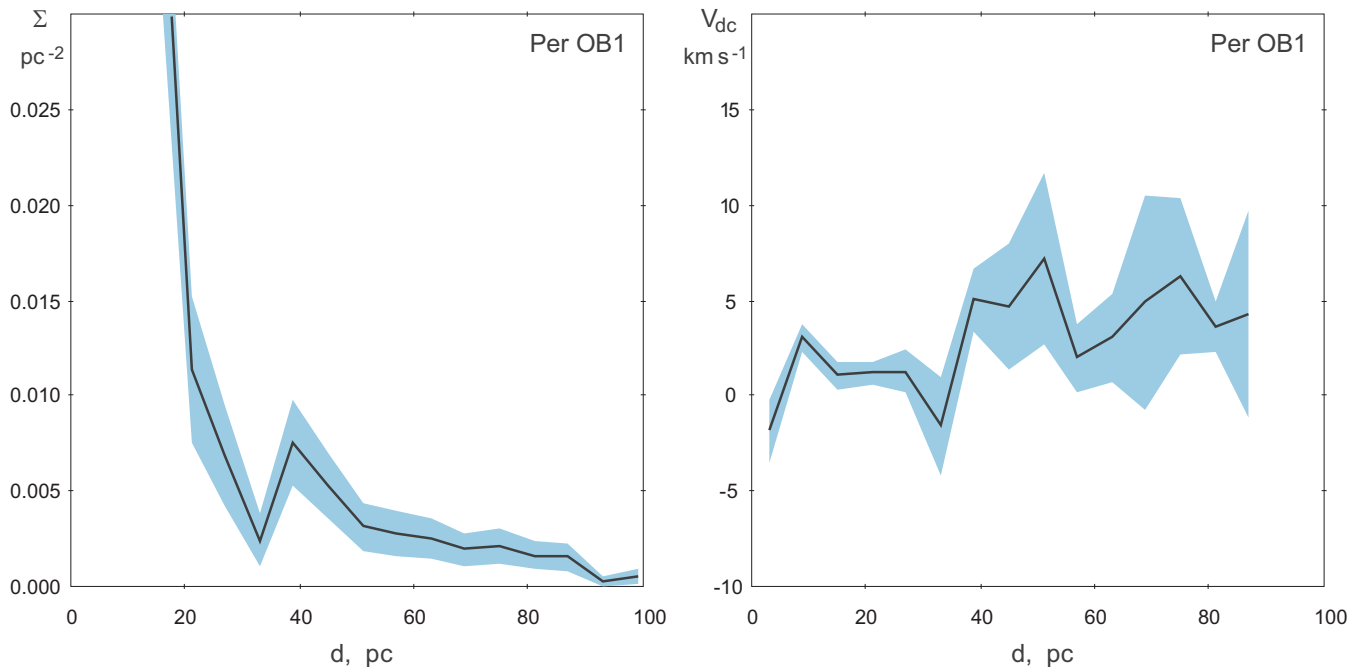


**Figure 7.** (a) Distribution of OB-stars inside the Per OB1 association averaged in thin annuli. The distribution of stars in the sky-plane was divided into 6 pc-wide annuli of radius  $d$  with the centres coincident with the centre of the association. The horizontal and vertical axes measure the distance from the centre,  $d$ , and the surface density of stars,  $\Sigma$ , respectively. The uncertainties due to Poisson noise are shown in gray (colored blue in the online article). We can see the existence of a secondary maximum at the distance 40 pc from the centre of the association. (b) Dependence of the velocity of expansion,  $V_{dc}$ , averaged in thin annuli on the distance  $d$ . The velocity  $V_{dc}$  is the relative corrected velocity in the direction connecting the centre of the association with the star. The velocity of expansion at the distance of the secondary maximum appears to be  $5.0 \pm 1.7 \text{ km s}^{-1}$ . The scatter due to root-mean-square errors in determination of average velocities in each annulus is shown in gray (colored blue in the online article).

## 5 ACKNOWLEDGEMENTS

We thank the anonymous referee for fruitful discussion. This work has made use of data from the European Space Agency (ESA) mission *Gaia* (<https://www.cosmos.esa.int/gaia>), processed by the *Gaia* Data Processing and Analysis Consortium (DPAC, <https://www.cosmos.esa.int/web/gaia/dpac/consortium>). Funding for the DPAC has been provided by national institutions, in particular the institutions participating in the *Gaia* Multilateral Agreement. This research has made use of the VizieR catalogue access tool, CDS, Strasbourg, France. The original description of the VizieR service was published by Ochsenbein, Bauer & Marcout (2000).

## REFERENCES

- Aldoretta E. J., et al., 2015, *AJ*, 149, 26  
 Ambartsumian V. A., 1949, *Soviet Astron. Zhurn.*, 26, 3  
 Arenou F., et al., 2018, *A&A*, 616, 17  
 Barbier-Brossat M., Figon P., 2000, *A&AS*, 142, 217  
 Baumgardt H., Kroupa P., 2007, *MNRAS*, 380, 1589  
 Blaauw A., 1964, *ARA&A*, 2, 213  
 Blaha C., Humphreys R. M., 1989, *AJ*, 98, 1598  
 Boily C. M., Kroupa P., 2003a, *MNRAS*, 338, 665  
 Boily C. M., Kroupa P., 2003b, *MNRAS*, 338, 673  
 Bressan A., Marigo P., Girardi L., Salasnich B., Dal Cero C., Rubele S., Nanni A., 2012, *MNRAS*, 427, 127  
 Brown A. G. A., Dekker G., de Zeeuw P. T., 1997, *MNRAS*, 285, 479  
 Brown A. G. A., et al., 2018, *A&A*, 616, A1  
 Cantat-Gaudin T., et al., 2019, *A&A*, 626, 17  
 Castor J., McCray R., Weaver R., 1975, *ApJ*, 200, L107  
 Chen H.-R., et al., 2019, *ApJ*, 875, 24  
 Colín P., Vázquez-Semadeni E., Gómez G. C., 2013, *MNRAS*, 435, 1701  
 Dale J. E., Ercolano B., Bonnell I. A., 2012, *MNRAS*, 427, 2852  
 Dambis A. K., Melnik A. M., Rastorguev A. S., 2001, *Astron. Lett.*, 27, 58  
 Dias W. S., Alessi B. S., Moitinho A., Lépine J. R. D., 2002, *A&A*, 389, 871  
 Efremov Yu. N., Sitnik T. G., 1988, *Soviet Astron. Lett.*, 14, 347  
 Elmegreen B. G., 1983, *MNRAS*, 203, 1011  
 Elmegreen B. G., Lada C. J., 1977, *ApJ*, 214, 725  
 ESA 1997, The HIPPARCOS and TYCHO catalogues. Astrometric and photometric star catalogues derived from the ESA HIPPARCOS Space Astrometry Mission, ESA SP, 1200  
 Evans N. J., et al., 2009, *ApJS*, 181, 321  
 Franco J., Shore S. N., Tenorio-Tagle G., 1994, *ApJ*, 436, 795  
 Fujii M. S., Portegies Zwart S., 2011, *Sci.*, 334, 1380  
 Gaia Collaboration, et al., 2016 *A&A*, 595, A1  
 Garcia P., Bronfman L., Nyman L.-A., Dame T. M., Luna A., 2014, *ApJS*, 212, 2

- Hills J. G., 1980, *ApJ*, 225, 986  
 Jordi C., et al., 2010 *A&A*, 523, A48  
 Katz D., et al., 2018, *A&A*, 616, A11  
 Kauffmann J., Pillai Th., Goldsmith P., 2013, *ApJ*, 779, 185  
 Kim J.-G., Kim W.-T., Ostriker E. C., 2016, *ApJ*, 819, 137  
 Kounkel M., et al., 2018, *AJ*, 156, 84  
 Kroupa P., 2002, *Sci*, 295, 82  
 Kroupa P., Aarseth S., Hurley J., 2001, *MNRAS*, 321, 699  
 Krumholz M. R., Matzner C. D., McKee C. F., 2006, *ApJ*, 653, 361  
 Larson R. B., 1981, *MNRAS*, 194, 809  
 Lindegren L., 2018, Gaia technical note GAIA-C3-TN-LU-LL-124, <https://www.cosmos.esa.int/web/gaia/ll-124>  
 Lindegren L., 2019, arXiv:1906.09827  
 Lindegren L., et al., 2016, *A&A*, 595, A4  
 Lindegren L., et al., 2018, *A&A* 616, A2  
 Lozinskaya T. A., 1999, *ASP Conference Series*, 168, 427  
 Lozinskaya T. A., Sitnik T., 1988, *Sov. Astron. Lett.*, 14, 100  
 Madsen S., Dravins D., Lindegren L., 2002, *A&A*, 381, 446  
 McKee C. F., 1989, *ApJ*, 345, 782  
 Melnik A. M., 2019, *MNRAS*, 485, 2106  
 Melnik A. M., Dambis A. K., 2009, *MNRAS*, 400, 518  
 Melnik A. M., Dambis A. K., 2017, *MNRAS*, 472, 3887  
 Melnik A. M., Dambis A. K., 2018, *Astron. Rep.*, 62, 997  
 Melnik A. M., Dambis A. K., 2020, in preparation  
 Melnik A. M., Efremov Yu. N., 1995, *Astron. Lett.*, 21, 10  
 Michalik D., Lindegren L., Hobbs D., 2015, *A&A*, 574, 115  
 Myers P. C., Dame T. M., Thaddeus P., Cohen R. S., Silverberg R. F., Dwek E., Hauser M. G., 1986, *ApJ*, 301, 398  
 Ochsenbein F., Bauer P., Marcout J., 2000, *A&AS*, 143, 23.  
 Pecaut M. J., Mamajek E. E., 2016, *MNRAS*, 461, 794  
 Riess A. G., et al., 2018, *ApJ*, 861, 126  
 Sanders D. B., Scoville N. Z., Solomon P. M., 1985, *ApJ*, 289, 373  
 Sitnik T. G., Melnik A. M., 1996, *Astron. Lett.*, 22, 422  
 Slesnick C. L., Hillenbrand L. A., Massey P., 2002, *ApJ*, 576, 880  
 Stassun K. G., Torres G., 2018, *ApJ*, 862, 61  
 Vine S. G., Bonnell I. A., 2003, *MNRAS*, 342, 314  
 Ward J. L., Kruijssen J. M. D., 2018, *MNRAS*, 475, 5659  
 Weaver R., McCray R., Castor J., Shapiro P., Moore R., 1977, *ApJ*, 218, 377  
 Wright N. J., Mamajek E. E., 2018, *MNRAS*, 476, 381  
 Yalyalieva L. N., Chemel A. A., Glushkova E. V., Dambis A. K., Klinichev A. D., 2018, *Astroph. Bull.*, 73, 335  
 Zamora-Aviles M., Vazquez-Semadeni E., Colin P., 2012, *ApJ*, 751, 77  
 Zinnecker H., Yorke H. W., 2007, *ARA&A*, 45, 481  
 (Sct OB2), HD 192445 (Cyg OB3), HD 192281 (Cyg OB8), HD 212043 (Cep OB2), HDE 240331 (Cas OB2), BD +59 70 (Cas OB4), BD +62 68 (Cas OB4), HILTNER 74 (Cas OB7), BD +60 261 (Cas OB8), HD 12323 (Per OB1), BD +60 512 (Cas OB6), HD 73634 (Vela OB1), HD 94024 (Car OB1), HD 102248 (Cru OB1), HD 112272 (Cen OB1).

## 5.1 Appendix

Here is the list of 17 stars of OB-associations with the absolute values of the relative velocities,  $V'_l$  or  $V'_b$ , greater than  $50 \text{ km s}^{-1}$ , which were excluded from our consideration in the study of the expansion of OB-associations (section 3.3): HD 163065 (Sgr OB5), HD 166937A (Sgr OB1), HD 172488